Proceedings of 20th International Congress on Acoustics, ICA 2010

23–27 August 2010, Sydney, Australia

The fast multipole BEM for low-frequency acoustic problems based on degenerate boundary formulation

Yosuke Yasuda (1), Takuya Oshima (2), Tetsuya Sakuma (3), Arief Gunawan (4) and Takayuki Masumoto (4)

(1) Department of Architecture, Faculty of Engineering, Kanagawa University, Rokkakubashi 3-27-1, Kanagawa-ku, Yokohama 221-8686, Japan
(2) Department of Civil Engineering and Architecture, Faculty of Engineering, Niigata University, 8050 Ninocho, Ikarashi, Niigata-city, Niigata 950-2181, Japan
(3) Department of Socio-Cultural Environmental Studies, Graduate School of Frontier Sciences, The University of Tokyo, 5-1-5 Kashiwanoha, Kashiwa-shi, Chiba 277-8563, Japan
(4) CYBERNET SYSTEMS CO.,LTD., FUJISOFT Bldg. 3 Kanda-neribeicho, Chiyoda-ku, Tokyo 101-0022, Japan

PACS: 43.55.Ka, 43.58.Ta

ABSTRACT

The fast multipole boundary element method (FMBEM), which is an efficient BEM with the use of the fast multipole method (FMM), is known to have instability at low frequencies when the well-known diagonal form for translation of multipole/local coefficients is employed. To overcome this problem, we have already developed a low-frequency FMBEM (LF-FMBEM), which is based on the original multipole expansion theory with translation techniques proposed by Gumerov and Duraiswami for avoiding the low-frequency instability. In the present paper, the degenerate boundary formulation, which is often referred to as the dual BEM, is discussed in the framework of the LF-FMBEM. The degenerate boundary formulation enables not only analyzing degenerate boundary models which have unknowns on both sides of the boundaries, but also avoiding well-known fictitious eigenfrequency difficulties for exterior problems. A concrete computational procedure of the LF-FMBEM based on the degenerate boundary formulation is described in details, which results in $O(N)$ operation counts and memory requirements. The computational accuracy and efficiency are validated through numerical experiments. Moreover, practically appropriate numerical settings on truncation numbers for multipole/local expansion coefficients and the lowest level for the hierarchical cell structure used in the FMM are investigated. Numerical results and computational efficiency of the LF-FMBEM are compared with those of the high-frequency FMBEM (HF-FMBEM), in which the diagonal form is employed.

INTRODUCTION

The boundary element method (BEM), which has been widely used in the field of acoustics, has a well-known drawback with computational efficiency. The BEM requires $O(N^3)$ operation count with direct solvers or $O(N^2)$ with appropriate iterative solvers, and $O(N^2)$ memory requirement, where N is the degree of freedom (DOF), because of the linear system with the dense matrix. This makes the BEM hardly applicable to large-scale problems. To overcome this problem, many studies have been conducted on the use of the fast multipole method (FMM) [8, 18]. In the field of acoustics, today we can see many studies and applications of the FMM to the BEM for the Helmholtz fields [1, 3, 7, 10, 20–22, 25–27]. This advanced BEM, known as the fast multipole BEM (FMBEM) can reduce both the operation count and the memory requirement to $O(N^a \log^b N)$, where $1 \leq a \leq 2$ and $b \geq 0$ depending on the geometry of the problem and the implementation.

In the FMM or the FMBEM, efficient translations of multipole and local expansion coefficients are much important. For three-dimensional Helmholtz fields, the diagonal form proposed by Rokhlin [17] has been widely adopted for efficient translation of multipole and local expansion coefficients. However, it is well known that this diagonal form causes numerical instability at low frequencies. Hence, the FMBEM with the diagonal form (high-frequency FMBEM: HF-FMBEM) gives inaccurate results when the dimensionless wavenumber normalized by the representative size of the analysis object is too small.

To avoid this instability at low frequencies, some techniques not based on Rokhlin's diagonal form have been proposed for translation of expansion coefficients [4, 9, 11, 12]. In recent years, not only the FMBEM with the use of these efficient translation techniques (low-frequency FMBEM: LF-FMBEM) [1], but also hybrid FMBEMs using both of the HF-FMM and the LF-FMM [3, 10] have been developed. However, the applicability of the LF-FMM to various formulations has not been fully discussed. Application of the LF-FMM to the degenerate boundary formulation, which is referred to as the dual BEM [6, 23], will be especially significant because the dual BEM can analyze degenerate boundary models which have unknowns on both sides of the boundaries, and avoid well-known fictitious eigenfrequency difficulties for exterior problems [14, 16]. Moreover, it has been reported [16] that the convergence of iterative solvers for the dual BE formulation is much faster than the formulation by Burton and Miller [2].

In the present paper, we provide concrete computational procedures for the degenerate boundary formulation of the LF-FMBEM for the Helmholtz fields. Through the formal estimation of the computational efficiency, we clarify the effects of

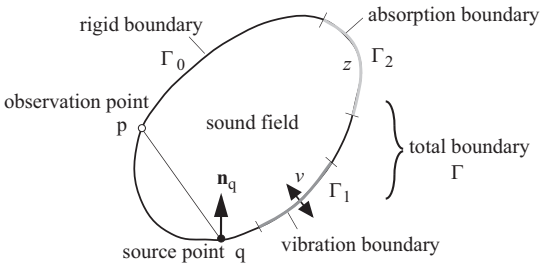

Figure 1: A sound field with three kinds of boundary.

the DOF, the truncation number of multipole and local expansions, and the lowest level of the hierarchical cell structure, on the entire computational efficiency of the LF-FMBEM based on the degenerate boundary formulation. The findings from the estimation are confirmed through numerical experiments.

OUTLINE OF BEM

Boundary conditions

Figure 1 shows a sound field satisfying the three-dimensional Helmholtz equation. Three kinds of locally-reactive boundary conditions are assumed as follows:

$$\frac{\partial p(\mathbf{r}_q)}{\partial n_q} = \begin{cases} 0 & q\in\Gamma_0 \ \text{(rigid)} \\ j\omega\rho v(\mathbf{r}_q) & q\in\Gamma_1 \ \text{(vibration)} \\ -jkp(\mathbf{r}_q)/z(\mathbf{r}_q) & q\in\Gamma_2 \ \text{(absorption)} \end{cases}, \quad (1)$$

where p is the sound pressure, v is the normal component of the surface velocity, z is the acoustic impedance ratio, ρ is the medium density, k is the wavenumber, ω is the angular frequency, and $\partial/\partial n_q$ is the normal derivative at a point q on the boundary.

Singular formulation

In a field satisfying the three-dimensional Helmholtz equation, the sound pressure at a point p on a smooth boundary Γ is represented using the Kirchhoff-Helmholtz integral equation

$$\frac{1}{2}p(\mathbf{r}_p) = \int_\Gamma \left(p(\mathbf{r}_q)\frac{\partial G(\mathbf{r}_p,\mathbf{r}_q)}{\partial n_q} - \frac{\partial p(\mathbf{r}_q)}{\partial n_q} G(\mathbf{r}_p,\mathbf{r}_q) \right) dS. \quad (2)$$

Here we omit the sound pressure by direct sources in the field. G is the three-dimensional free-space Green's function given by

$$G(\mathbf{r}_p,\mathbf{r}_q) = \frac{\exp(jkr_{pq})}{4\pi r_{pq}}, \quad (3)$$

where $r_{pq} = |\mathbf{r}_q - \mathbf{r}_p|$ is the distance between points p and q. Discretization of Eq. (2) with the boundary conditions Eq. (1) leads to the following system of linear equations:

$$(\mathbf{B}+\mathbf{C}-\mathbf{E})\mathbf{p} = j\omega\rho\mathbf{A}\mathbf{v}, \quad (4)$$

where $\mathbf{p}$ is the sound pressure vector (unknown), $\mathbf{v}$ is the velocity vector (given). The entries of the coefficient matrices are represented by

$$E_{ij} = \frac{1}{2}\delta_{ij}, \quad (5)$$

$$A_{ij} = \int_{\Gamma_1} N_j(\mathbf{r}_q) G(\mathbf{r}_i,\mathbf{r}_q) dS, \quad (6)$$

$$B_{ij} = \int_{\Gamma} N_j(\mathbf{r}_q) \frac{\partial G(\mathbf{r}_i,\mathbf{r}_q)}{\partial n_q} dS, \quad (7)$$

$$C_{ij} = \frac{jk}{z(\mathbf{r}_i)} \int_{\Gamma_2} N_j(\mathbf{r}_q) G(\mathbf{r}_i,\mathbf{r}_q) dS, \quad (8)$$

where δ is Kronecker's delta, $\mathbf{r}_i$ is the position vector of the i-th node, N_j is the interpolation function of the j-th node. Sound pressures on the nodes are obtained by solving Eq. (4). Since the system matrix $(\mathbf{B}+\mathbf{C}-\mathbf{E})$ is dense, the operation count to solve Eq. (4) is of $O(N^3)$ with direct solvers, where N is the number of nodes. Even if an efficient iterative solver is used, the count of $O(N^2)$ is required due to matrix-vector multiplications $(\mathbf{B}+\mathbf{C}-\mathbf{E})\mathbf{p}$. The memory requirement is also of $O(N^2)$ to store the dense matrices. All the remaining formulations described in this section have the same drawback of efficiency, which is a serious obstacle for solving large scale problems.

Hypersingular formulation

The following hypersingular-type integral equation is obtained by differentiating Eq. (2) with respect to the normal at a point p on the boundary.

$$\frac{1}{2}\frac{\partial p(\mathbf{r}_p)}{\partial n_p} = \int_\Gamma \left(p(\mathbf{r}_q)\frac{\partial^2 G(\mathbf{r}_p,\mathbf{r}_q)}{\partial n_p \partial n_q} - \frac{\partial p(\mathbf{r}_q)}{\partial n_q}\frac{\partial G(\mathbf{r}_p,\mathbf{r}_q)}{\partial n_p} \right) dS. \quad (9)$$

Discretization of the above equation with the boundary conditions Eq. (1) leads to the following system of equations:

$$(\mathbf{B}'+\mathbf{C}'+\mathbf{H})\mathbf{p} = j\omega\rho(\mathbf{A}'+\mathbf{F})\mathbf{v}, \quad (10)$$

The entries of the coefficient matrices are represented by

$$F_{ij} = \frac{1}{2}\delta_{ij}\Big|_{\Gamma_1}, \quad (11)$$

$$H_{ij} = \frac{jk}{2z(\mathbf{r}_i)}\delta_{ij}\Big|_{\Gamma_2}, \quad (12)$$

$$A'_{ij} = \int_{\Gamma_1} N_j(\mathbf{r}_q)\frac{\partial G(\mathbf{r}_i,\mathbf{r}_q)}{\partial n_i} dS, \quad (13)$$

$$B'_{ij} = \int_{\Gamma} N_j(\mathbf{r}_q)\frac{\partial^2 G(\mathbf{r}_i,\mathbf{r}_q)}{\partial n_i \partial n_q} dS, \quad (14)$$

$$C'_{ij} = \frac{jk}{z(\mathbf{r}_i)}\int_{\Gamma_2} N_j(\mathbf{r}_q)\frac{\partial G(\mathbf{r}_i,\mathbf{r}_q)}{\partial n_i} dS. \quad (15)$$

Sound pressures on the nodes are obtained by solving Eq. (10).

Degenerate boundary formulation

All of the above formulations with standard boundary elements having values only on one side present some difficulties for the analysis of thin bodies, such as plates. A boundary of zero thickness Λ called the degenerate boundary is introduced to overcome this problem. Integral equations Eqs. (2) and (9) can be rewritten with the degenerate boundary as follows:

$$\frac{1}{2}\hat{p}(\mathbf{r}_p) = \int_\Lambda \left(\tilde{p}(\mathbf{r}_q)\frac{\partial G(\mathbf{r}_p,\mathbf{r}_q)}{\partial n_q} - \frac{\partial \tilde{p}(\mathbf{r}_q)}{\partial n_q} G(\mathbf{r}_p,\mathbf{r}_q) \right) dS, \quad (16)$$

$$\frac{1}{2}\frac{\partial \hat{p}(\mathbf{r}_p)}{\partial n_p} = \int_\Lambda \left(\tilde{p}(\mathbf{r}_q)\frac{\partial^2 G(\mathbf{r}_p,\mathbf{r}_q)}{\partial n_p \partial n_q} - \frac{\partial \tilde{p}(\mathbf{r}_q)}{\partial n_q}\frac{\partial G(\mathbf{r}_p,\mathbf{r}_q)}{\partial n_p} \right) dS, \quad (17)$$

where $\hat{p} = p^+ + p^-$, $\tilde{p} = p^+ - p^-$, p^+ and p^- are the sound pressures on the both sides of the degenerate boundary. In this formulation n_p and n_q denote the normals for the p^+ side. The following two systems of equations with unknown vectors of both sides of the boundary $\mathbf{p}^+$ and $\mathbf{p}^-$ are obtained by discretizing Eqs. (16) and (17) with boundary conditions for both sides.

$$(\mathbf{B}+\mathbf{C}^+-\mathbf{E})\mathbf{p}^+ - (\mathbf{B}-\mathbf{C}^-+\mathbf{E})\mathbf{p}^- = j\omega\rho\mathbf{A}(\mathbf{v}^+ + \mathbf{v}^-), \quad (18)$$

$$(\mathbf{B}'+\mathbf{C}'^+ + \mathbf{H}^+)\mathbf{p}^+ - (\mathbf{B}'-\mathbf{C}'^- + \mathbf{H}^-)\mathbf{p}^- = j\omega\rho\left((\mathbf{A}'+\mathbf{F})\mathbf{v}^+ + (\mathbf{A}'-\mathbf{F})\mathbf{v}^-\right), \quad (19)$$

where the superscripts $^+$ and $^-$ denote values for the p^+ and p^- sides, respectively. Sound pressures on both sides of the degenerate boundary are obtained by solving the following system composed of Eqs. (18) and (19).

$$\begin{bmatrix} \mathbf{B}+\mathbf{C}^+-\mathbf{E} & -\mathbf{B}+\mathbf{C}^--\mathbf{E} \\ \mathbf{B}'+\mathbf{C}'^++\mathbf{H}^+ & -\mathbf{B}'+\mathbf{C}'^--\mathbf{H}^- \end{bmatrix} \begin{bmatrix} \mathbf{p}^+ \\ \mathbf{p}^- \end{bmatrix} = j\omega\rho \begin{bmatrix} \mathbf{A} & \mathbf{A} \\ \mathbf{A}'+\mathbf{F} & \mathbf{A}'-\mathbf{F} \end{bmatrix} \begin{bmatrix} \mathbf{v}^+ \\ \mathbf{v}^- \end{bmatrix}. \quad (20)$$

This formulation is often referred to as the dual BEM [6]. It has been reported that this formulation enables avoiding fictitious eigenfrequency difficulties for the analysis of exterior problems [14, 16]. For this purpose, the characteristic impedance of the propagation medium has to be given to the imaginary surface inside of the body. This technique is similar to that proposed by Hirosawa, *et al.*[13] In the latter technique, however, an analyzed body is treated as a shell with finite thickness using standard boundary elements, and fictitious eigenfrequencies are controlled not to be in the analysis frequency region by reducing the thickness of the shell. Hence there is a limitation that the size of boundary elements cannot be so large compared to the thickness of the shell to ensure the computational accuracy. On the other hand, the dual BEM does not have such a limitation because it uses boundaries of zero thickness. Moreover, it has been reported that when an iterative method was used to solve the system of equations, the convergence of the dual BEM was much faster than that of Burton-Miller formulation [16], which generally produces an ill-conditioned matrix.

When neither side of the degenerate boundary is absorptive, Eq. (19) can be simplified to the following system [23]. The DOF of this system is half of that of Eq. (20).

$$\mathbf{B}'\tilde{\mathbf{p}} = j\omega\rho\left((\mathbf{A}'+\mathbf{F})\mathbf{v}^+ + (\mathbf{A}'-\mathbf{F})\mathbf{v}^-\right), \quad (21)$$

where $\tilde{\mathbf{p}}$ is the sound pressure difference vector (unknown). Sound pressure differences between both sides of the boundary are obtained by solving Eq. (21).

Hereafter, we refer to the formulation of Eq. (20) as the dual degenerate boundary formulation, and that of Eq. (21) as the single degenerate boundary formulation.

LF-FMBEM WITH DEGENERATE BOUNDARIES

Outline of FMBEM

Here we briefly describe the general outline of the FMBEM. Refer to Refs. [11, 15, 20], *etc.* for more details.

Matrix-vector multiplication using multipole/local expansions

The FMBEM accelerates the matrix-vector multiplications which appear in the iterative process of the BEM matrix solution by replacing the multiplications with the multipole and local expansion operations. The replacement is possible because what the multiplications do is physically a summation of potentials contributed from all boundary elements. As will be shown in the subsequent sections, the summation can be performed efficiently by calculating multipole and local expansions in conjunction with coefficient translations for hierarchically grouped boundary elements. The translation technique, which is the key to an effective LF-FMBEM algorithm, will be paid a special attention.

Translation of coefficients

Translation of the expansion coefficients at a point $\mathbf{r}_1$ to those at another point $\mathbf{r}_2$ can be expressed in matrix-vector forms as follows:

$$\text{M2M translation} : \mathbf{M}(\mathbf{r}_2) = (\mathbf{R}|\mathbf{R})(\mathbf{t})\mathbf{M}(\mathbf{r}_1), \quad (22)$$

$$\text{M2L translation} : \mathbf{L}(\mathbf{r}_2) = (\mathbf{S}|\mathbf{R})(\mathbf{t})\mathbf{M}(\mathbf{r}_1), \quad (23)$$

$$\text{L2L translation} : \mathbf{L}(\mathbf{r}_2) = (\mathbf{R}|\mathbf{R})(\mathbf{t})\mathbf{L}(\mathbf{r}_1), \quad (24)$$

where $\mathbf{t} = \mathbf{r}_2 - \mathbf{r}_1$, $\mathbf{M}$ and $\mathbf{L}$ are vectors of multipole and local expansion coefficients with the truncation number N_c for the infinite summation, respectively, $(\mathbf{R}|\mathbf{R})$ and $(\mathbf{S}|\mathbf{R})$ are dense matrices for translation of expansion coefficients.

Grouping with hierarchical cell structures

A hierarchical cell structure is introduced for multilevel grouping of sources and observation points. Figure 2 shows a boundary and a hierarchical cell structure in two dimensions. A cube (a square in two dimensions) circumscribing the whole boundary is determined as a root cell (level $l = 0$), which is divided into eight child cubes ($l = 1$). Each divided cube is again divided in turn ($l = 2, 3, \cdots, L$). In this figure the lowest level number $L = 4$. The concept of hierarchical cell structures is common for LF- and HF-FMBEM, including definition of relationship between cells. Refer to Refs. [11, 20], *etc.* for more details.

Translation techniques

Since the matrices in Eqs. (22), (23) and (24) are dense, translations explicitly using these matrices (*e.g.* those using Wigner 3j-symbols [5]) require $O(N_c^5)$ operation counts [12]. To avoid this inefficiency, many researchers have used the diagonal forms [17]. However, these forms have a problem of instability at low frequencies. Various techniques have been proposed for efficient translation of coefficients for low frequency problems. Most of these techniques theoretically reduce the operation counts to $O(N_c^3)$ [3, 4, 9, 11, 12]. In the present paper, we adopted a technique using the Taylor expansions [11] for M2M and L2L translations, and the rotation - coaxial translation - backrotation (RCR) technique [3, 9, 11, 12] with recurrence relations [11, 12] for M2L translation, based on some numerical experiments [28].

Algorithm of LF-FMBEM based on degenerate boundary formulation

Multipole expansions of matrix entries

Eqs. (6), (7) and (8) can be expressed as the following multipole expansions at a point λ:

$$\begin{bmatrix} A_{ij} \\ B_{ij} \\ C_{ij} \end{bmatrix} = jk \sum_{n=0}^{N_c-1} \sum_{m=-n}^{n} S_n^m(\mathbf{r}_{\lambda i}) \begin{bmatrix} \alpha^m_{n(\lambda j)} \\ \beta^m_{n(\lambda j)} \\ \gamma^m_{n(\lambda j)} \end{bmatrix}, \quad (25)$$

where

$$\alpha^m_{n(\lambda j)} = \int_{\Gamma_1} N_j(\mathbf{r}_q) R_n^{-m}(\mathbf{r}_{\lambda q}) dS, \quad (26)$$

$$\beta^m_{n(\lambda j)} = \int_{\Gamma} \frac{\partial}{\partial n_q} N_j(\mathbf{r}_q) R_n^{-m}(\mathbf{r}_{\lambda q}) dS, \quad (27)$$

$$\gamma^m_{n(\lambda j)} = \frac{jk}{z(\mathbf{r}_i)} \int_{\Gamma_2} N_j(\mathbf{r}_q) R_n^{-m}(\mathbf{r}_{\lambda q}) dS. \quad (28)$$

$\partial R_n^{-m}/\partial n_q$, which is required for computation of β_n^m, can be calculated using the following relation

$$\frac{\partial}{\partial n_q}\mathbf{R} = k\mathbf{D_t}\mathbf{R}, \quad (29)$$

where $\mathbf{D_t}$ is a matrix representation of a differential operator (Eq. (7.3.33) in Ref. [11], with the direction of derivative $\mathbf{t} = \mathbf{n}_q$).

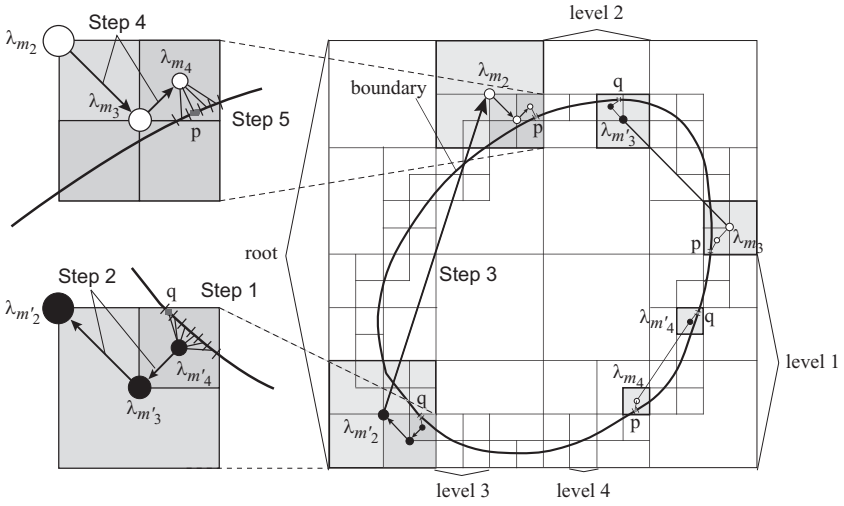

Figure 2: 2-D hierarchical cell structure (the lowest level number $L = 4$) and diagram of steps 1 to 5.

Computational procedures

Here we present concrete computational procedures for calculation of matrix-vector products for both of the dual and single degenerate boundary formulations. The procedures consist of six steps. Steps 2, 3 and 4 are completely the same as those for the singular and hypersingular formulations. Also see Fig. 2.

Dual degenerate boundary formulation Here we deal with Eq. (20).

Step 1. Compute the multipole expansion coefficients $M^m_{n\,(m_L)}$ at the center point λ_{m_L} of each cell m_L at the lowest level L, by

$$\begin{bmatrix} M^{m(\mathrm{p})}_{n\,(m_L)} \\ M^{m(\mathrm{v})}_{n\,(m_L)} \end{bmatrix} = jk \sum_{j\in \mathtt{G}_{m_L}} \begin{bmatrix} (\beta^m_{n\,(\lambda_{m_L} j)} + \gamma^{m+}_{n\,(\lambda_{m_L} j)}) p^+_j - (\beta^m_{n\,(\lambda_{m_L} j)} - \gamma^{m-}_{n\,(\lambda_{m_L} j)}) p^-_j \\ \alpha^m_{n\,(\lambda_{m_L} j)} \hat{v}_j \end{bmatrix}, \quad (30)$$

where $\mathtt{G}_{m_L}$ denotes the set of all elements in the cell m_L, the superscripts $^+$ and $^-$ denote the values on one and the other sides of the degenerate boundary, $\hat{v}_j = v^+_j + v^-_j$, and the superscripts (p) and (v) denote that the coefficients are for the left and the right hand sides of Eq. (4), respectively. In the following, we omit these superscripts when the equations for both become identical.

Step 2 (M2M). Compute the multipole expansion coefficients $M^m_{n\,(m_l)}$ of each cell m_l at the next higher level l, by the M2M translation

$$\mathbf{M}_{(m_l)} = \sum_{m_{l+1}\in \mathtt{C}_{m_l}} (\mathbf{R}|\mathbf{R})(\mathbf{r}_{\lambda_{m_{l+1}}\lambda_{m_l}}) \mathbf{M}_{(m_{l+1})}, \quad (31)$$

where $\mathtt{C}_{m_l}$ denotes the child cell set, which consists of child cells of the cell m_l. This computation is executed at each level in the upward order ($l = L-1, L-2, \ldots, 2$). Here we adopt sparse matrix decompositions (the Taylor expansions) of the dense matrix $(\mathbf{R}|\mathbf{R})$ [11], which allows the operation count of the translation to reduce to $O(N_c^3)$. Eq. (31) can be rewritten as:

$$\mathbf{M}_{(m_l)} = \sum_{m_{l+1}\in \mathtt{C}_{m_l}} \sum_{n=0}^{N_t} \frac{(kt)^n}{n!} \mathbf{D}^n_{\mathbf{t}} \mathbf{M}_{(m_{l+1})}, \quad (32)$$

where $\mathbf{D}_{\mathbf{t}}$ is the same as in Eq. (29), $t = |\mathbf{t}|$ and $\mathbf{t} = \mathbf{r}_{\lambda_{m_{l+1}}\lambda_{m_l}}$. In the present paper we adopt $N_t = N_c/2$ based on a numerical experiment [28].

Step 3 (M2L). Compute the local expansion coefficients $L^m_{n\,(\mathtt{I}m_l)}$ of each cell m_l at each level ($l = 2, 3, \ldots, L$), by the M2L translation

$$\mathbf{L}_{(\mathtt{I}m_l)} = \sum_{m'_l\in \mathtt{T}_{m_l}} (\mathbf{S}|\mathbf{R})(\mathbf{r}_{\lambda_{m'_l}\lambda_{m_l}}) \mathbf{M}_{(m'_l)}, \quad (33)$$

where $\mathtt{T}_{m_l}$ denotes the interaction cell set, which consists of the cells which are not neighbors of m_l but whose parents are neighbors of the parent cell of m_l. For computational efficiency, Eq. (33) is decomposed to the following three steps by the RCR technique [3, 9, 11, 12].

- rotation

$$\begin{aligned} \mathbf{M}_{(\mathrm{coax})(m'_l)} &= \mathbf{Rot}(Q(\alpha,\beta,0))\mathbf{M}_{(m'_l)} \\ &= \mathbf{Rot}(B(\beta))\mathbf{Rot}^{-1}(A(\alpha))\mathbf{M}_{(m'_l)}, \end{aligned} \quad (34)$$

- coaxial translation

$$\mathbf{L}^{(m'_l)}_{(\mathrm{coax})(\mathtt{I}m_l)} = (\mathbf{S}|\mathbf{R})_{(\mathrm{coax})}(r_{\lambda_{m'_l}\lambda_{m_l}} \mathbf{i}_{\hat{z}}) \mathbf{M}_{(\mathrm{coax})(m'_l)}, \quad (35)$$

- backrotation

$$\mathbf{L}_{(\mathtt{I}m_l)} = \sum_{m'_l\in \mathtt{T}_{m_l}} \mathbf{Rot}(A(\alpha))\mathbf{Rot}(B(\beta)) \mathbf{L}^{(m'_l)}_{(\mathrm{coax})(\mathtt{I}m_l)}, \quad (36)$$

where $Q(\alpha,\beta,\gamma) = A(\gamma)B(\beta)A^{\mathrm{T}}(\alpha)$ is the rotation matrix, $\mathbf{Rot}(Q)$ is the translation matrix for rotation, $(\mathbf{S}|\mathbf{R})_{(\mathrm{coax})}(\mathbf{t})$ is the translation matrix for coaxial translation, and $\mathbf{i}_{\hat{z}}$ is the unit vector in z-axis. The direction of $\mathbf{r}_{\lambda_{m'_l}\lambda_{m_l}}$ that points from $\lambda_{m'_l}$ to λ_{m_l} is referred to as $(\theta,\varphi) = (\beta,\alpha)$ in the spherical coordinates. We adopt techniques using recurrence relations to calculate translation matrices in Eqs. (34), (35) and (36) [11, 12]. The operation counts for calculation and multiplication of these matrices are of $O(N_c^3)$.

Step 4 (L2L). Compute the local expansion coefficients $L^m_{n\,(\mathtt{U}m_{l+1})}$ of each cell m_{l+1} at the next lower level $l+1$, by the L2L translation

$$\mathbf{L}_{(\mathtt{U}m_{l+1})} = (\mathbf{R}|\mathbf{R})(\mathbf{r}_{\lambda_{m_l}\lambda_{m_{l+1}}})(\mathbf{L}_{(\mathtt{I}m_l)} + \mathbf{L}_{(\mathtt{U}m_l)}), \quad (37)$$

where $L^m_{n\,(\mathtt{I}m_l)}$ is computed in Step 3, and $L^m_{n\,(\mathtt{U}m_2)} = 0$ if $l = 2$. This computation is executed in the downward order at each level ($l = 2, 3, \ldots, L-1$). Here we adopt the same translation technique as in Step 2. Eq. (37) can be rewritten as:

$$\mathbf{L}_{(\mathtt{U}m_{l+1})} = \sum_{n=0}^{N_t} \frac{(kt)^n}{n!} \mathbf{D}^n_{\mathbf{t}} (\mathbf{L}_{(\mathtt{I}m_l)} + \mathbf{L}_{(\mathtt{U}m_l)}), \quad (38)$$

where $\mathbf{t} = \mathbf{r}_{\lambda_{m_l}\lambda_{m_{l+1}}}$.

Step 5. Compute the far influences on each node within the cell m_L. The influences $\phi^{\mathrm{SF}}_{\mathrm{F},i}$ in the singular formulation and $\phi^{\mathrm{HF}}_{\mathrm{F},i}$ in the hypersingular formulation are calculated by Eqs. (39) and (40), respectively.

$$\phi^{\mathrm{SF}}_{\mathrm{F},i} = \sum_{n=0}^{N_c-1}\sum_{m=-n}^{n} L^m_{n\,(m_L)} R^m_n(\mathbf{r}_{\lambda_{m_L} i}). \tag{39}$$

$$\begin{aligned}\phi^{\mathrm{HF}}_{\mathrm{F},i} &= \sum_{n=0}^{N_c-1}\sum_{m=-n}^{n} \frac{\partial}{\partial n_i}\left(L^m_{n\,(m_L)} R^m_n(\mathbf{r}_{\lambda_{m_L} i})\right) \\ &= \sum_{n=0}^{N_c-1}\sum_{m=-n}^{n} \tilde{L}^m_{n\,(m_L)} R^m_n(\mathbf{r}_{\lambda_{m_L} i}).\end{aligned} \tag{40}$$

$\tilde{\mathbf{L}}_{(m_L)}$, which is a vector representation of $\tilde{L}^m_{n\,(m_L)}$, can be computed by

$$\tilde{\mathbf{L}}_{(m_L)} = k\mathbf{D}_{\mathbf{t}}\mathbf{L}_{(m_L)}, \tag{41}$$

where the direction of derivative $\mathbf{t} = \mathbf{n}_i$ in $\mathbf{D}_{\mathbf{t}}$.

Step 6. Compute the near influences $\phi^{\mathrm{SF}}_{\mathrm{N},i}$ in the singular formulation and $\phi^{\mathrm{HF}}_{\mathrm{N},i}$ in the hypersingular formulation on each node, resulting from the effect of the elements in the neighbor cell set at the lowest level L, by

$$\begin{bmatrix} \phi^{\mathrm{SF,p}}_{\mathrm{N},i} \\ \phi^{\mathrm{SF,v}}_{\mathrm{N},i} \end{bmatrix} = \sum_{m'_L \in \mathtt{N}_{m_L}} \sum_{j \in \mathtt{G}_{m'_L}} \begin{bmatrix} (B_{ij} + C^+_{ij} - E_{ij}) p^+_j - (B_{ij} - C^-_{ij} + E_{ij}) p^-_j \\ A_{ij}\hat{v}_j \end{bmatrix}, \tag{42}$$

$$\begin{bmatrix} \phi^{\mathrm{HF,p}}_{\mathrm{N},i} \\ \phi^{\mathrm{HF,v}}_{\mathrm{N},i} \end{bmatrix} = \sum_{m'_L \in \mathtt{N}_{m_L}} \sum_{j \in \mathtt{G}_{m'_L}} \begin{bmatrix} (B'_{ij} + C'^+_{ij} + H^+_{ij}) p^+_j - (B'_{ij} - C'^-_{ij} + H^-_{ij}) p^-_j \\ (A'_{ij} + F_{ij}) v^+_j + (A'_{ij} - F_{ij}) v^-_j \end{bmatrix}. \tag{43}$$

where $\mathtt{N}_{m_L}$ denotes the neighbor cell set, which consists of m_L itself and neighboring cells of m_L.

Finally, compute the total influence on each node by adding the far and the near influences, $\phi^{\mathrm{SF}}_i = \phi^{\mathrm{SF}}_{\mathrm{F},i} + \phi^{\mathrm{SF}}_{\mathrm{N},i}$ and $\phi^{\mathrm{HF}}_i = \phi^{\mathrm{HF}}_{\mathrm{F},i} + \phi^{\mathrm{HF}}_{\mathrm{N},i}$, which give the matrix-vector products in Eq. (20).

Single degenerate boundary formulation Here we deal with Eq. (21). Each step described above is simplified as follows.

Step 1. Eq. (30) is simplified as follows:

$$\begin{bmatrix} M^{m(\mathrm{p})}_{n\,(m_L)} \\ M^{m(\mathrm{v})}_{n\,(m_L)} \end{bmatrix} = jk \sum_{j \in \mathtt{G}_{m_L}} \begin{bmatrix} \beta^m_{n\,(\lambda_{m_L} j)} \tilde{p}_j \\ \alpha^m_{n\,(\lambda_{m_L} j)} \hat{v}_j \end{bmatrix}. \tag{44}$$

Step 5. Same as Eq. (40).

Step 6. Eq. (43) is simplified as follows:

$$\begin{bmatrix} \phi^{\mathrm{p}}_{\mathrm{N},i} \\ \phi^{\mathrm{v}}_{\mathrm{N},i} \end{bmatrix} = \sum_{m'_L \in \mathtt{N}_{m_L}} \sum_{j \in \mathtt{G}_{m'_L}} \begin{bmatrix} B'_{ij}\tilde{p}_j \\ (A'_{ij} + F_{ij}) v^+_j + (A'_{ij} - F_{ij}) v^-_j \end{bmatrix}. \tag{45}$$

COMPUTATIONAL EFFICIENCY OF LF-FMBEM

Here we estimate the operation counts and memory requirements for the LF-FMBEM in accordance with the computational procedures for the dual degenerate boundary formulation presented above. We focus the difference in computational efficiency between singular and dual degenerate boundary formulations, especially when the same boundary element mesh is used for calculations. The DOFs for the singular formulation and single degenerate boundary formulation are identical to the number of nodes N, whereas that for the dual degenerate boundary formulation is $2N$. In the following, N is the number of nodes, M is the average number of nodes in a cell at the lowest level L, M_l is the number of cells at a level l ($M_l \sim (2^a)^l$ when nodes are a-dimensionally distributed in a space), N_c is the truncation number for multipole and local expansions (assumed to be constant independently of level l), $S = \sum_{n=0}^{N_c-1}(2n+1) = N_c^2$ is the number of multipole and local expansion coefficients, and $N_t \sim N_c$ [11] is the truncation number for the Taylor expansions in Steps 2 and 4. $M_L = N/M$ and $L \sim \log(N/M)$.

Operation counts

Setup process

To reduce total operation counts for the LF-FMBEM, coefficients unnecessary to be iteratively computed should be computed before iterative matrix-vector multiplications. The operation counts only for steps 1 and 6 (Eqs. (30), (42) and (43)) are greater than those for the singular formulation. The estimation results showed that the total operation count for the setup process $\overline{C}$ is approximately $O(N)$ and decreases as the lowest level L increases, like the singular formulation. Here we omit the estimation since the operation counts for this part is usually smaller than those for iterative process.

Iterative process

Operation counts for steps in the iterative process are listed below. Here $\overline{C_i}$ denotes the operation count for Step i.

- Step 1. $C_1 \sim e_b NS \sim e_b N N_c^2$.
- Step 2. $C_2 \sim \sum_{l=2}^{L-1} M_{l+1} N_c^3 \sim N_c^3 \frac{N}{M}$.
- Step 3. $C_3 \sim \sum_{l=2}^{L} 3IM_l N_c^3 \sim 3IN_c^3 \frac{N}{M}$, where $I \le 6^3 - 3^3 = 189$ is the average number of interaction cells.
- Step 4. $C_4 \sim C_2$.
- Step 5. $C_5 \sim C_1$.
- Step 6. $C_6 \sim e_b NMR$.

e_b is 1 for the singular formulation or 2 for the dual degenerate boundary formulation. The total operation count for a single iteration C is expressed as the following equation, which depends on N, N_c and M.

$$C \sim \sum_{i=1}^{6} C_i \sim N\left(e_b b_1 M + b_2 N_c^3 \frac{1}{M} + e_b b_3 N_c^2\right), \tag{46}$$

where b_i are machine and implementation dependent. If $N \gg N_c^3$ and if N_c and M are chosen independently of N, the operation count for the iterative process is $O(N)$.

The value of M at which C is minimized, $M_{C\mathrm{opt}}$, is expressed as follows, from $\partial C/\partial M \sim 0$:

$$M_{C\mathrm{opt}} \sim \sqrt{\frac{b_2}{e_b b_1} N_c^3}. \tag{47}$$

This indicates that the lowest cell level $L_{C\mathrm{opt}}$ at which C is minimized depends on the truncation number N_c for multipole and local expansions, and that $L_{C\mathrm{opt}}$ decreases as N_c increases. If N_c is constant, $M_{C\mathrm{opt}}$ is also constant independently of N.

Hence, $L_{C\mathrm{opt}}$ can be chosen beforehand based on the value of $M_{C\mathrm{opt}}$.

Memory requirements

Like the HF-FMBEM, the LF-FMBEM stores coefficients computed in the setup process on memory, instead of the dense system matrix of the linear equations. Memory requirements for these coefficients are listed below. Here E_a denotes the memory requirement for a.

- For p and v, $E_{pv} \sim 2N$.
- For $\alpha_{m,n}^{\lambda_{m_L} j}$ and $\beta_{m,n}^{\lambda_{m_L} j} + \gamma_{m,n}^{\lambda_{m_L} j}$ in Step 1, $E_{\alpha\beta\gamma} \sim 2e_b NS \sim 2e_b NN_\mathrm{c}^2$.
- For $\mathbf{Rot}(B(\beta))$ and $(\mathbf{S}|\mathbf{R})_{(\mathrm{coax})}$ in Step 3, $E_{\mathbf{Rot}} \sim I_\mathrm{r} N_\mathrm{c}^3$ and $E_{(\mathbf{S}|\mathbf{R})} \sim I_\mathrm{c}(L-1)N_\mathrm{c}^3$.
- For $j_n(kr_{\lambda_{m_L} i})Y_n^m(\theta_{\lambda_{m_L} i})$ in Step 5, $E_{jY} \sim NS \sim NN_\mathrm{c}^2$.
- For A_{ij} and $B_{ij} + C_{ij}$ in Step 6, $E_{ABC} \sim 2e_b NMR$.

The total memory requirement E is expressed as the following equation, which depends on N, N_c and M.

$$\begin{aligned} E &\sim E_{pv} + E_{\alpha\beta\gamma} + E_{\mathbf{Rot}} + E_{(\mathbf{S}|\mathbf{R})} + E_{jY} + E_{ABC} \\ &\sim N(c_1 M + e_c c_2 N_\mathrm{c}^2 + c_3) + N_\mathrm{c}^3 \left(c_4 \log \frac{N}{M} + c_5 \right), \end{aligned} \tag{48}$$

where $1 < e_c < 2$, and c_i are machine and implementation dependent. If $N \gg N_\mathrm{c}^3$ and if N_c and M are chosen independently of N, the total memory requirement is approximately $O(N)$.

The following relation can be obtained from Eq. (48):

$$\frac{\partial E}{\partial M} \sim c_1 N - \frac{c_4 N_\mathrm{c}^3}{M}. \tag{49}$$

This value is minimized with $M = 1$. If $N \gg N_\mathrm{c}^3$, then $\partial E/\partial M \big|_{M=1} > 0$. In this case E is monotonically increasing within $M \geq 1$ and takes the minimum at $M = 1$. Namely, the total memory requirement decreases as the lowest level L increases. This is the same for the singular formulation.

NUMERICAL RESULTS

A sphere model

We investigate the relation of the truncation number N_c for expansions and the lowest cell level L to computational accuracy and efficiency of the LF-FMBEM through numerical experiments with a sphere model, for which the theoretical solutions are known. An exterior problem of the sphere is calculated using the dual degenerate boundary formulation. The characteristic impedance of the medium is given to the inside surface of the sphere to avoid fictitious eigenfrequency difficulties [13, 14, 16].

Theoretical solution [24]

Consider a sphere the center of which is at the origin with a radius a, as shown in Fig. 3. The vibration velocity v of the surface is given as follows:

$$v(\theta) = \begin{cases} v_0 & (0 \leq \theta \leq \alpha) \\ 0 & (\alpha < \theta \leq \pi) \end{cases}, \tag{50}$$

where θ is the angle from the positive direction of the z-axis. The sound pressure $p(r,\theta)$ outside the sphere ($a \leq r$) is expressed as:

$$\begin{aligned} p(r,\theta) \quad = \quad & \frac{j\rho c v_0}{2} \sum_{n=0}^{\infty} [P_{n-1}(\cos\alpha) - P_{n+1}(\cos\alpha)] \\ & \cdot \frac{h_n^{(1)}(kr)}{h_n^{(1)\prime}(ka)} P_n(\cos\theta), \end{aligned} \tag{51}$$

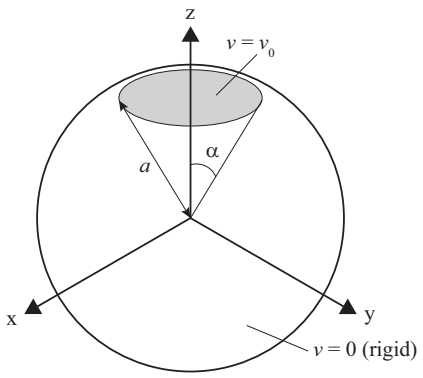

Figure 3: An analysis model of a sphere.

where c is the speed of sound, and P_n are the Legendre polynomials. In this numerical experiment, $\rho = 1.225$ [kg/m^3], $c = 340$ [m/s], $a = 0.125$ [m], $v_0 = 1$ [m/s] and $\alpha = 20$ [deg].

Numerical setup

Consider three boundary element meshes: the element sizes of Cases 1, 2 and 3 are about 1/40, 1/20 and 1/10 of the analysis wavelength of 5 kHz, respectively. Case n has about 4 times as many nodes as Case $n+1$, where $n = 1, 2$. The numbers of nodes N are 126 628 for Case 1, 31 200 for Case 2, and 7 768 for Case 3. Constant elements are used. GPBiCG [29] is used as the iterative solver with preconditioning ILUT$(10^{-6}, 100)$ [19]. The following equation is used as the stopping criterion:

$$\frac{\|\mathbf{r}_i\|_2}{\|\mathbf{b}\|_2} = \frac{\|\mathbf{b} - \mathbf{A}\mathbf{x}_i\|_2}{\|\mathbf{b}\|_2} < \varepsilon, \tag{52}$$

where $\mathbf{A}$ and $\mathbf{b}$ are the system matrix and the right hand side vector, respectively, $\mathbf{x}_i$ and $\mathbf{r}_i$ are the approximate solution vector and the residual vector at i-th iteration, respectively, and $\|\cdot\|_2$ is the 2-norm. Here $\varepsilon = 10^{-9}$ is used. In the following, $L_{\min} = 2$ and $L_{\max}$ denotes the largest L, at which $M < 10$. The computation is executed with DELL Precision690 (Intel(R) Xeon(R) Processor X5355 2.66 GHz, 32.0 GB RAM, Windows XP Prefessional x64 edition).

Results and discussion

Effect of the truncation number for expansions Figure 4 shows sound pressure level distributions on the exterior surface of the sphere at 5 kHz. Results using the singular formulation (SF) are also shown for reference. It can be confirmed that the fictitious eigenfrequency difficulties are not seen with the dual degenerate boundary formulation for all cases. Results show some discrepancy from theoretical ones with $N_\mathrm{c} \leq 10$ in all cases. Table 1 shows relative errors ε_r from theoretical results, calculated by the following equation:

$$\varepsilon_\mathrm{r} = \sqrt{\frac{\sum_n |p_{\mathrm{cal}}(\theta_n) - p_{\mathrm{th}}(\theta_n)|^2}{\sum_n |p_{\mathrm{th}}(\theta_n)|^2}}, \tag{53}$$

where $p_{\mathrm{th}}(\theta_n)$ and $p_{\mathrm{cal}}(\theta_n)$ are the theoretical and calculated values of the surface sound pressure at an angle θ_n, respectively. In all cases, the errors generally converge at $N_\mathrm{c} = 12$. This was the same for interior problems of the same sphere. Hereafter, we adopt $N_\mathrm{c} = 12$ based on this investigation.

Effect of the lowest cell level Table 2 shows computational time and required memory at 5 kHz. Regarding the computational time, it can be pointed out that the time for the setup process decreases as the lowest cell level L increases, and that

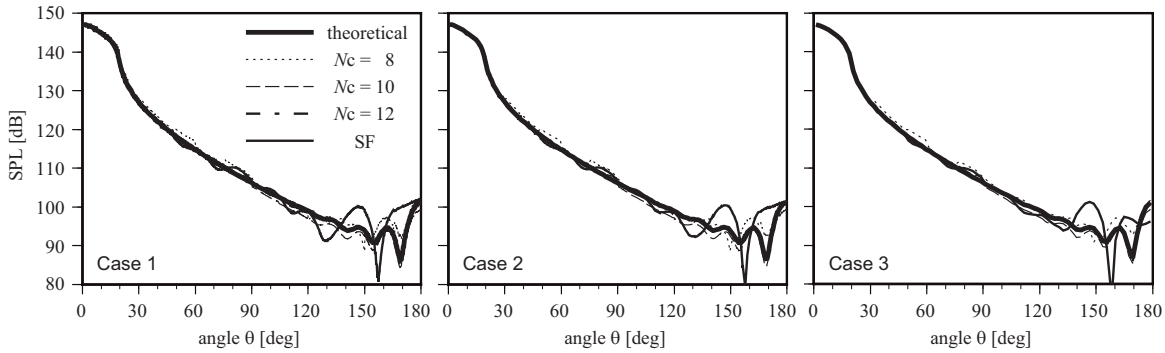

Figure 4: Sound pressure level distributions (Case 2, f = 5 [kHz], $L = L_{\max}$): (a) on the interior surface of the sphere, and (b) on the exterior surface.

Table 1: Relative error ε_r of the exterior surface of the sphere (f = 5 [kHz], $L = L_{\max}$).

N_c	8	10	12	14	16	20
Case 1	1.52×10^{-2}	6.07×10^{-3}	5.17×10^{-3}	4.89×10^{-3}	4.88×10^{-3}	4.88×10^{-3}
Case 2	1.59×10^{-2}	6.15×10^{-3}	5.26×10^{-3}	4.91×10^{-3}	4.90×10^{-3}	4.90×10^{-3}
Case 3	1.86×10^{-2}	9.87×10^{-3}	9.14×10^{-3}	9.23×10^{-3}	9.25×10^{-3}	9.23×10^{-3}

Table 2: Performance for the exterior problem of the sphere (f = 5 [kHz], N_c = 12).

Case	N	L	M	Memory [MB]	Time [sec] Setup	Iterative (w. ILUT)	Total	1 iteration (w.o. ILUT)	Iteration
1	126 628	4	109	1.60×10^4	1 459	3 256	4 715	28.7	68
		5	27	5.99×10^3	420	3 884	4 304	52.0	68
		6	7	3.67×10^3	162	11 858	12 020	156.6	74
2	31 200	2	557	1.50×10^4	1 496	3 059	4 555	13.9	48
		3	114	3.88×10^3	351	662	1 013	6.6	51
		4	27	1.47×10^3	102	738	840	12.7	51
		5	7	9.02×10^2	40	2 087	2 126	40.3	50
3	7 768	2	138	1.06×10^3	95	147	242	1.5	38
		3	28	3.64×10^2	25	129	155	2.8	38
		4	7	2.25×10^2	10	347	357	9.7	34

the time for a single iteration of the iterative process is the shortest with $M \approx 100$ independently of N. These findings accord with the conclusions of the previous estimation of computational efficiency, and the same tendency was shown as the interior problems of the same sphere. These facts indicate that the optimum L for the time of a single iteration ($L_{C\text{opt}}$) depends only on M, not on the formulation or the number of nodes. If M remains approximately constant across the cases, the times of a single iteration approximately follow $O(N)$, whereas the total computational times do not. This is because the number of iteration slightly increases with N. Since the time of the iterative process in general depends on the number of iteration, the optimum L for the total time ($L_{T\text{opt}}$) is between that for the time of a single iteration ($L_{C\text{opt}}$) and that for the setup process ($L_{\overline{C}\text{opt}} = L_{\max}$), depending on the number of iteration. As for the memory requirements, findings from numerical results accord with the conclusions of the previous estimation; the memory requirements for both of the interior and exterior problems decrease as the lowest cell level L increases, and they follow $O(N)$ as long as M remains approximately constant across the cases.

A train coach model

We analyze the exterior sound field around a train coach as an example of large-scale noise problems with degenerate boundaries. We compare the results using the HF-FMBEM and the LF-FMBEM.

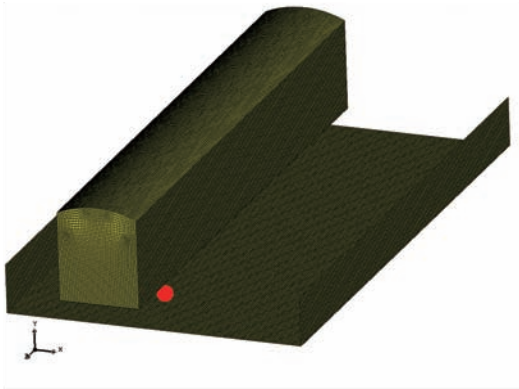

Figure 5: A boundary element mesh of the analysis model (DOF is 220 288).

Analysis model

Figure 5 shows a boundary element mesh of an analysis model. A coach is located above an elevated bridge, which is 5 m above an infinite rigid plane. A point source is located at the position of a wheel. The length of the coach is 20 m. We use 148 544 constant degenerate boundary elements, 71 744 elements of which compose the coach with rigid outside surfaces and absorptive inside ones (the acoustic impedance ratio is 1). The rest of the elements are for the elevated bridge and both

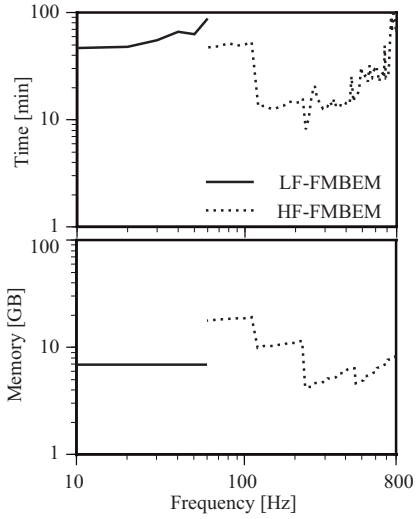

Figure 6: Calculation performance for the train model.

sides of them are rigid. Hence, the DOF is 220 288, and a mixed formulation of the single and dual degenerate boundary ones is used for this model. We analyze the sound field below and at 60 Hz using the LF-FMBEM, and at and above 60 Hz using the HF-FMBEM. This problem is symmetrical because the image elements with respect to the infinite rigid plane have to be included, which makes the DOF twice. Here we efficiently calculate this symmetrical problem using a technique proposed in Ref. [25]. The computer and numerical settings for the LF-FMBEM are the same as the sphere problems, except for $\varepsilon = 10^{-3}$. The lowest cell level for the LF-FMBEM is $L = 6$, which approximately minimizes the computational time. As for the HF-FMBEM, the lowest cell level L is set to satisfy $kD_L > \pi/2$, where D_L is the diagonal length of the cell at the level L, to ensure the computational accuracy. The other numerical items are identical with those in Ref. [27].

Results and discussion

Table 3 shows sound pressure level distributions on the boundaries: at 30 and 60 Hz by the LF-FMBEM, and at 60 and 800 Hz by the HF-FMBEM. The results by both methods agree well at 60 Hz. Figure 6 shows the computational time and the required memory. The computational times for both methods are compatible at low frequencies (below 100 Hz), and the required memory for the LF-FMBEM is much smaller than that for the HF-FMBEM, less than 7 GB. This indicates highly good computational efficiency of the LF-FMBEM. The memory for the standard BEM is more than 776 GB only for the system matrix.

CONCLUSIONS

We have discussed the computational procedures and efficiency for the degenerate boundary formulation of the fast multipole BEM for low-frequency problems (LF-FMBEM). We have estimated the operation counts and memory requirements based on the presented computational procedures. Findings from the estimation have been confirmed through numerical experiments. We have investigated the effects of the truncation number N_c for multipole and local expansions and the lowest level L of the hierarchical cell structure on the computational accuracy and efficiency. Main conclusions are as follows.

- $N_c \geq 12$ was required to avoid computational errors caused by the multipole and local expansions, at least for non-absorptive sphere problems.
- The operation counts both for the setup and iterative processes and the total memory requirement are of $O(N)$, like the singular formulation, where N is the number of nodes.
- The average number $M_{C_{\text{opt}}}$ of nodes in a cell at the lowest cell level $L_{C_{\text{opt}}}$, at which the operation count for the iterative process is minimized, is approximately constant, independently of N. Hence, $L_{C_{\text{opt}}}$ can be chosen beforehand from $M_{C_{\text{opt}}}$.
- The total memory requirement decreases as the lowest cell level L increases.
- The LF-FMBEM based on the degenerate boundary formulation is a highly efficient method as well as the HF-FMBEM based on the same formulation, especially at low frequencies.

REFERENCES

[1] M. S. Bapat, L. Shen, and Y. J. Liu. “Adaptive fast multipole boundary element method for three-dimensional half-space acoustic wave problems”. *Eng. Anal. Bound. Elem.* 33 (2009), pp. 1113–1123.

[2] A. J. Burton and G. F. Miller. “The application of integral equation methods to the numerical solution of some exterior boundary value problems”. *Roy. Soc. London, Ser. A* 323 (1971), pp. 201–210.

[3] H. Cheng et al. “A wideband fast multipole method for the Helmholtz equation in three dimensions”. *J. Comput. Phy.* 216 (2006), pp. 300–325.

[4] E. Darve and P. Havé. “Efficient fast multipole method for low-frequency scattering”. *J. Comput. Phys.* 197 (2004), pp. 341–363.

[5] M. A. Epton and B. Dembart. “Multipole translation theory for the three-dimensional Laplace and Helmholtz equations”. *SIAM J. Sci. Comput.* 16 (1995), pp. 865–897.

[6] O. von Estorff (Ed.) *Boundary Elements in Acoustics: Advances and Applications*. WIT Press, Boston, 2000.

[7] M. Fischer, U. Gauger, and L. Gaul. “A multipole Galerkin boundary element method for acoustics”. *Eng. Anal. Bound. Elem.* 28 (2004), pp. 155–162.

[8] L. Greengard. *The rapid evaluation of potential fields in particle systems*. The MIT press, London, 1988.

[9] L. Greengard et al. “Accelerating fast multipole methods for the Helmholtz equation at low frequencies”. *IEEE Comput. Sci. Eng.* 5 (1998), pp. 32–38.

[10] N. A. Gumerov and R. Duraiswami. “A broadband fast multipole accelerated boundary element method for the three dimensional Helmholtz equation”. *J. Acoust. Soc. Am.* 125 (2009), pp. 191–205.

[11] N. A. Gumerov and R. Duraiswami. *Fast multipole methods for the Helmholtz equation in three dimensions*. Elsevier, 2004.

[12] N. A. Gumerov and R. Duraiswami. “Recursions for the computation of multipole translation and rotation coefficients for the 3-D Helmholtz equation”. *SIAM J. Sci. Comput.* 25 (2003), pp. 1344–1381.

[13] K. Hirosawa, T. Ishizuka, and K. Fujiwara. “A simple method avoiding non-nniqueness in the boundary element method for acoustic scattering problem”. *J. Acoust. Soc. Am.* 125 (2009), pp. 2838–2846.

[14] Y. Kosaka and T. Sakuma. “Boundary element analysis using thin plate modeling –On calculation of a thin plate with different boundary conditions for both surfaces– (in Japanese)”. *Proc. Autumn Meet. Acoust. Soc. Jpn.* Sendai, 2005, pp. 979–980.

Table 3: The SPL distributions of the train coach model. The amplitude of the point source is 1 Pa at 1 m away.

Freq. [Hz]	30	60	800
LF-FMBEM	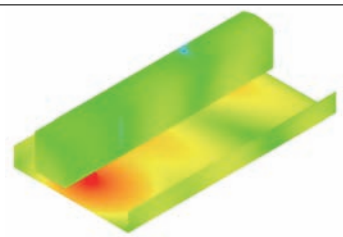	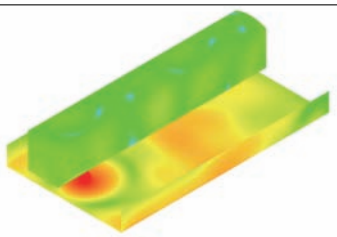	N/A
HF-FMBEM	N/A	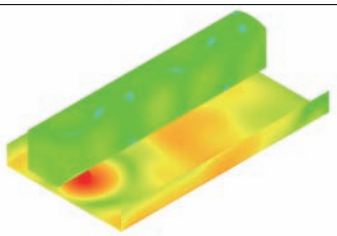	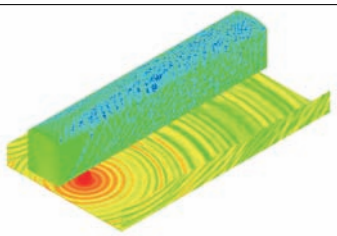

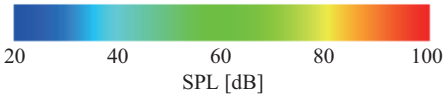

[15] S. Marburg and B. Nolte (Ed.) *Computational acoustics of noise propagation in fluids –finite and boundary element methods*. Springer-Verlag, Berlin, 2008. Chap. 12.

[16] T. Masumoto et al. "HRTF caulculation in the full audible frequency range using FMBEM". *Proc. 19th Int'l Cong. Acoust.* COM-06-012. Madrid, 2007.

[17] V. Rokhlin. "Diagonal forms of translation operators for the Helmholtz equation in three dimensions". *Appl. and Comput. Harm. Anal.* 1 (1993), pp. 82–93.

[18] V. Rokhlin. "Rapid solution of integral equations of classical potential theory". *Comput. Phys.* 60 (1983), pp. 187–207.

[19] Y. Saad. "ILUT: a dual threshold incomplete LU factorization". *Numer. Linear Algebra* 1 (1994), pp. 387–402.

[20] T. Sakuma and Y. Yasuda. "Fast multipole boundary element method for large-scale steady-state sound field analysis. Part I: setup and validation". *Acta Acustica united with Acustica* 88 (2002), pp. 513–525.

[21] S. Schneider. "Application of fast methods for acoustic scattering and radiation problems". *J. comput. Acoust.* 11 (2003), pp. 387–401.

[22] L. Shen and Y. J. Liu. "An adaptive fast multipole boundary element method for three-dimensional acoustic wave problems based on the Burton-Miller formulation". *Comput. Mech.* 40 (2007), pp. 461–472.

[23] T. Terai. "On calculation of sound fields around three dimensional objects by integral equation methods". *J. Sound Vib.* 69 (1980), pp. 71–100.

[24] E. G. Williams. *Fourier Acoustics*. Academic Press, London, 1999. Chap. 6.

[25] Y. Yasuda and T. Sakuma. "A Technique for plane-symmetric sound field analysis in the fast multipole boundary element method". *J. Comput. Acoust.* 13 (2005), pp. 71–85.

[26] Y. Yasuda and T. Sakuma. "An effective setting of hierarchical cell structure for the fast multipole boundary element method". *J. Comput. Acoust.* 13 (2005), pp. 47–70.

[27] Y. Yasuda and T. Sakuma. "Fast multipole boundary element method for large-scale steady-state sound field analysis. Part II: examination of numerical items". *Acta Acustica united with Acustica* 89 (2003), pp. 28–38.

[28] Y. Yasuda, T. Sakuma, and T. Oshima. "The fast multipole BEM for low-frequency calculation: investigation on translation of coefficients (in Japanese)". *Proc. Spring Meet. Acoust. Soc. Jpn*. 2009, pp. 1059–1062.

[29] S.-L. Zhang. "GPBi-CG: Generalized product-type methods based on Bi-CG for solving nonsymmetric linear systems". *SIAM J. Sci. Comput.* 18 (1997), pp. 537–551.